Ta thickness effect on field-free switching and spin–orbit torque efficiency in a ferromagnetically coupled Co/Ta/CoFeB trilayer

Zhongshu Feng(冯重舒)[1], Changqiu Yu(于长秋)[1,†], Haixia Huang(黄海侠)[1], Haodong Fan(樊浩东)[1], Mingzhang Wei(卫鸣璋)[1], Birui Wu(吴必瑞)[1], Menghao Jin(金蒙豪)[1], Yanshan Zhuang(庄燕山)[1], Ziji Shao(邵子霁)[1], Hai Li(李海)[1], Jiahong Wen(温嘉红)[1], Jian Zhang(张鉴)[2], Xuefeng Zhang(张雪峰)[2], Ningning Wang(王宁宁)[1], Sai Mu(穆赛)[1], and Tiejun Zhou(周铁军)[1,‡]

[1] *School of Electronics and Information Engineering, Hangzhou Dianzi University, Hangzhou* 310018, *China*

[2] *Second Affiliation Institute of Advanced Magnetic Materials, College of Materials and Environmental Engineering, Hangzhou Dianzi University, Hangzhou* 310018, *China*

(Received 8 September 2022; revised manuscript received 26 November 2022; accepted manuscript online 2 December 2022)

Current induced spin–orbit torque (SOT) switching of magnetization is a promising technology for nonvolatile spintronic memory and logic applications. In this work, we systematically investigated the effect of Ta thickness on the magnetic properties, field-free switching and SOT efficiency in a ferromagnetically coupled Co/Ta/CoFeB trilayer with perpendicular magnetic anisotropy. We found that both the anisotropy field and coercivity increase with increasing Ta thickness from 0.15 nm to 0.4 nm. With further increase of Ta thickness to 0.5 nm, two-step switching is observed, indicating that the two magnetic layers are magnetically decoupled. Measurements of pulse-current induced magnetization switching and harmonic Hall voltages show that the critical switching current density increases while the field-free switching ratio and SOT efficiency decrease with increasing Ta thickness. Both the enhanced spin memory loss and reduced interlayer exchange coupling might be responsible for the $\beta_{\rm DL}$ decrease as the Ta spacer thickness increases. The studied structure with the incorporation of a CoFeB layer is able to realize field-free switching in the strong ferromagnetic coupling region, which may contribute to the further development of magnetic tunnel junctions for better memory applications.

Keywords: spin–orbit coupling, interlayer exchange-coupling, field-free switching

PACS: 85.70.–w, 75.60.Jk, 75.70.Tj **DOI:** 10.1088/1674-1056/aca7e9

1. Introduction

With the rapid development of spintronics, current-induced spin–orbit torque (SOT) has been considered as one of the promising technologies for next generation memory and logic devices due to its ultra-low power consumption and ultra-fast operation speed.[1–3] When the charge current flows through the heavy metal (HM) layer with strong spin–orbit coupling a spin current can be generated due to the spin Hall effect (SHE)[2,4–6] and/or the Rashba effect.[7–9] The resulting spin current will inject into the adjacent ferromagnetic (FM) layer and switch the magnetization via the SOT.[10–13] Typically, an external magnetic field parallel to the current is required to induce deterministic magnetization switching, which is disadvantageous for miniaturization of the device.

Therefore, how to realize field-free switching and further improve the SOT efficiency have been the focus of research. Up to now, field-free switching of perpendicular magnetization has been demonstrated using a lateral wedge structure,[14–16] exchange bias,[14,17–19] tilted anisotropy,[20–23] and stacks with lateral or vertical symmetry breaking.[24,25] On the other hand, field-free switching of perpendicular magnetization has also been reported in T-type FM bilayer films, with in-plane and out-of-plane anisotropy, respectively, using interlayer exchange coupling.[22,23,26] However, there is a lack of detailed investigation into the effects of spacer thickness on field-free switching and, most importantly, SOT efficiency, especially for exchange-coupled FM bilayers that have both perpendicular anisotropy and high thermal stability, and therefore high-density memory applications.

In this work, we systematically studied field-free switching and SOT efficiency in perpendicularly magnetized Co and CoFeB bilayers, sandwiched by an ultrathin Ta layer with varied thickness, through which the interlayer exchange coupling (IEC) strength can be effectively tuned. It is found that the magnetic properties depend on the Ta thickness, and 0.5 nm Ta is able to magnetically decouple the two magnetic layers. The measurements of pulse-current induced magnetization switching and harmonic Hall voltages show that the critical switching current density increases, while the field-free switching ratio and SOT efficiency decrease with increasing Ta thickness. Both the enhanced spin memory loss and reduced IEC might be responsible for the decrease in $\beta_{\rm DL}$ as the Ta spacer thickness increases. The studied structure with the incorporation of a CoFeB layer is able to realize field-free switching in the strong FM coupling region, which may contribute to the further development of magnetic tunnel junctions for better mem-

†Corresponding author. E-mail: cqyu@hdu.edu.cn
‡Corresponding author. E-mail: tjzhou@hdu.edu.cn

© 2023 Chinese Physical Society and IOP Publishing Ltd

ory applications.

2. Experimental details

Ta(1)/Pt(5.5)/Co(1.2)/Pt(0.2)/Ta(t)/CoFeB(1)/MgO(2)/Ta(3) (in units of nanometers, from bottom to top) heterostructures (Fig. 1(a)) were deposited on thermally oxidized Si substrates by magnetron sputtering at a base vacuum better than 5×10^{-8} Torr. After completing deposition by a DC/RF magnetron sputtering system, the films were annealed at 300 °C for 30 min in a vacuum to enhance perpendicular magnetic anisotropy (PMA). The 1 nm Ta layer at the bottom is used as the seed layer and the 3 nm Ta layer at the top is used for isolation from the air and to protect the device. The sandwiched Ta layer with varied thickness, $t_{\rm Ta}$, between Co and CoFeB serves as the coupling-tuning layer, and provides better PMA for the upper CoFeB layer.[27] At the same time, the negative spin Hall angle of the bottom Pt layer provides an upward spin current. The two FM layers are composed of a Co layer and a CoFeB layer, both of which have PMA, so that the two FM layers are perpendicularly coupled together. Specifically, the bottom Co(1.2) layer has a stronger PMA with a $H_{\rm k}$ of 1.18 T (Fig. S1), and Pt(0.2) is used to further enhance the PMA of Co. The top CoFeB(1) has weaker PMA with a $H_{\rm k}$ of 0.55 T (Fig. S1), and MgO(1) is used to improve the PMA of CoFeB.

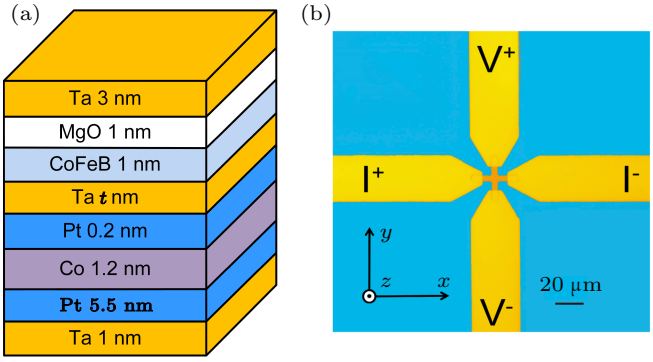


Fig. 1. (a) The stack structure of the films with varied $t_{\rm Ta}$. (b) Optical microscope image of the Hall bar and connection modes.

Then, the stacks were patterned into Hall bars with a size of 5 μm × 5 μm using photolithography and Ar ion etching. Ti(5)–Au(50) electrodes were employed to form a non-magnetic ohmic contact. The photolithography pattern and coordinate system are shown in Fig. 1(b). The current is applied in the x direction, the Hall voltage is extracted in the y direction and the z direction is perpendicular to the plane of the film. The measurements of anomalous Hall resistance, $R_{\rm AHE}$, were obtained by applying a magnetic field perpendicular to the film and using a Keithley 6221 current source and a SR830 lock-in amplifier. A magneto-optical Kerr effect (MOKE) system was applied to obtain the magnetic properties of the film. All the measurements were carried out at room temperature. A series of current pulses of varying amplitude with a pulse width of 30 μs were applied to the device to switch the magnetization. Between two consecutive pulses, a small current was used to record the Hall resistance. The SOT of this structure was examined by performing harmonic Hall voltage measurements, which are widely used to evaluate the magnitude and sign of the SOT.[28,29] An in-plane field, H_x, was applied in the x–z plane at a polar angle of $\theta_H = 3^\circ$; an AC, $I = I_0\sin(\omega t)$, was applied along the x axis, which generated an alternating SOT to oscillate the magnetic moment around H_x. Under the large in-plane external magnetic field, the Co layers and the CoFeB layers tilt toward the H_x direction and are modulated by AC effective SOT fields. Because of the high external magnetic field and strong FM coupling, the Co layers and the CoFeB layers become a single domain, and the second harmonic Hall resistance signal $R_{xy}^{2\omega}$ measured as a function of H_x can be expressed as[30]

$$R_{xy}^{2\omega} = \frac{R_{\rm AHE}}{2}\frac{H_{\rm DL}}{H_x - H_{\rm k}} + \frac{R_{\rm PHE}}{2}\frac{H_{\rm FL}}{H_x} + R_{\rm SSE+ANE+ONE}, \quad (1)$$

where $H_{\rm DL}$ and $H_{\rm FL}$ are the antidamping-like and field-like effective fields and $R_{\rm AHE}$ and $R_{\rm PHE}$ are the anomalous and planar Hall resistance, respectively. $R_{\rm SSE+ANE+ONE}$ is the contribution from the spin Seebeck (SSE) effect, anomalous Nernst effect (ANE) and ordinary Nernst effect (ONE). The merit of high-field second harmonic measurement is that it can distinguish the intrinsic SOT contribution from those of the thermal effects $R_{\rm ANE+SSE+ONE}$. To rule out any possible thermal contribution, the second harmonic Hall signal as a function of $1/(H_x - H_{\rm k})$ is plotted (see Fig. S2 in the supplementary materials). The intercept through a linear fit to the data is about 0.017 mΩ–0.021 mΩ, indicating a very small and negligible contribution from thermal effects. The magnetic anisotropy field $(H_{\rm k})$ is defined as the point where the normalized in-plane component of the magnetization $m_x = \sqrt{1-m_z^2}$ equals 0.98.[31]

3. Results and discussion

The MOKE measurements characterize the PMA for different $t_{\rm Ta}$ samples, as shown in Fig. 2(a). The FM coupling appears only in a narrow $t_{\rm Ta}$ spacer range (0.15 nm–0.4 nm). At $t_{\rm Ta} = 0.1$ nm, the film does not have a perpendicular easy axis. The coercivity increases with Ta thickness, from about 80 Oe at $t_{\rm Ta} = 0.15$ nm to about 150 Oe at $t_{\rm Ta} = 0.4$ nm. However, two-step switching appears at $t_{\rm Ta} = 0.5$ nm, indicating that the two magnetic layers (Co/Pt and CoFeB) are individually switched, and therefore magnetically decoupled. The square shape also confirms the PMA of the Co and CoFeB layers, and the gradient relationship of $M_{\rm s}$ and $H_{\rm k}$ of the two FM layers. We therefore mainly studied $t_{\rm Ta} = 0.15$ nm–0.4 nm for

SOT switching since we are mainly talking about the changes in the FM coupling intensity. Figure 2(b) also shows how H_k changes with Ta thickness. Clearly H_k follows the same trend as H_c when Ta thickness varies.

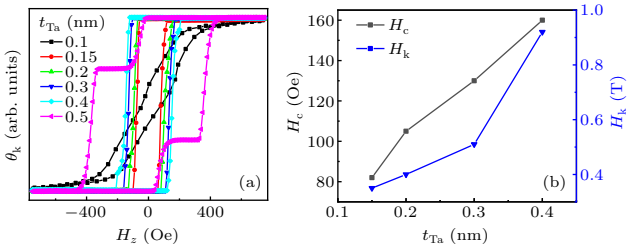


Fig. 2. (a) Hysteresis loops of the Co/Ta/CoFeB samples with varying thickness of Ta from 0.1 nm to 0.5 nm by MOKE. (b) Coercivity (H_c) and H_k as a function of t_{Ta}.

To investigate the effect of t_{Ta} on magnetization switching, we performed SOT-induced magnetization switching experiments. As shown in Fig. 3(a), we break the chiral symmetry by constructing the saturation magnetization and PMA gradient of the upper and lower FM layers with FM coupling. The anomalous Hall resistance R_{AHE} as a function of out-of-plane field H_z for various Ta thicknesses ($t_{Ta} = 0.1$ nm–0.5 nm) is shown in Fig. 3(b). R_{AHE} shows a negligible decrease ($\sim 0.1\ \Omega$) with increase in Ta thickness from 0.15 nm to 0.4 nm. This also indicates that the shunt effect of Ta does not play a dominant role in this structure.

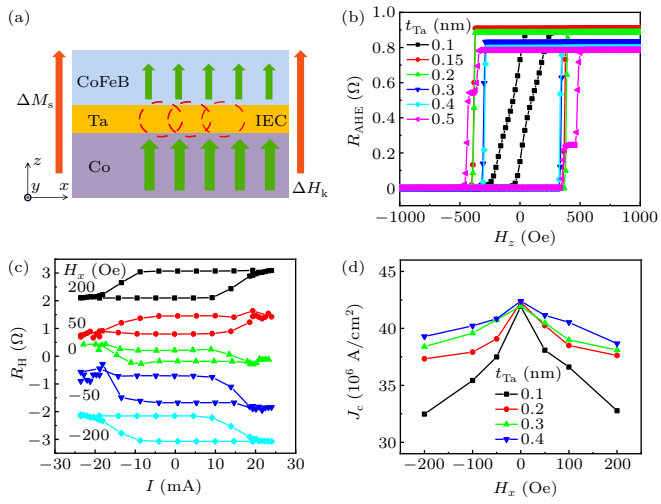


Fig. 3. (a) Schematic of the M_s and H_k gradient along the z direction that breaks the chiral symmetry, leading to field-free SOT switching. (b) The anomalous Hall resistance R_{AHE} as a function of out-of-plane field H_z for various Ta thicknesses ($t = 0.1$ nm–0.5 nm). (c) Current-induced SOT switching loops of $t_{Ta} = 0.15$ nm under different H_x. (d) The critical switching current density (J_c) as a function of the in-plane auxiliary field with various t_{Ta}. Here J_c is defined as the current density at which 50% switching happens.

As a result, in the strong FM coupling region ($t_{Ta} = 0.15$ nm), we observed field-free SOT switching as shown in Fig. 3(c). This field-free switching loop has the same polarity as in cases with a negative H_x. These results indicate the existence of an effective internal field that participates in the SOT switching process. In addition, similar results are also observed with t_{Ta} up to 0.4 nm. The M_s and H_k gradient (Fig. 3(a)) formed in our samples breaks the chiral symmetry and results in a dynamic noncollinear spin texture under current-driven SOT, leading to field-free switching of perpendicular magnetization, similar to what has been reported previously.[32–34] The critical switching current densities, J_c, at different external fields for varied t_{Ta} are summarized in Fig. 3(d). As expected, J_c decreases with increasing H_x, which is a typical feature of SOT-induced magnetization switching. Most importantly, J_c increases with Ta thickness until two magnetic layers are magnetically decoupled at $t_{Ta} = 0.5$ nm.

Figure 4(a) shows current-induced field-free magnetization switching loops with varied t_{Ta}. It can be seen that with the decrease of t_{Ta}, the field-free switching performance improves rapidly, which agrees well with the decrease of J_c mentioned above. Therefore, it can be concluded that a thinner Ta layer is favorable for magnetization switching. In addition, the switching ratio as a function of external magnetic field is summarized in Fig. 4(b). The field-free switching ratio given by the solid line shows a maximum switching ratio of 41% at 0.15 nm Ta when $H_x = 0$ Oe. The dashed line indicates that SOT switching disappears at $H_x = 15$ Oe when $t_{Ta} = 0.15$ nm and 0.2 nm, which corresponds to an equivalent effective field of -15 Oe along the charge-current direction. However, the equivalent effective field decreases to 6 Oe at Ta thicknesses of 0.3 nm and 0.4 nm.

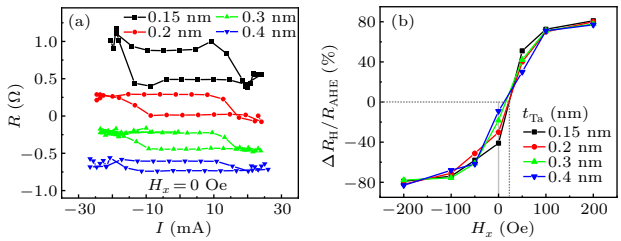


Fig. 4. (a) Current-induced field-free magnetization switching loops for varied t_{Ta}. (b) Switching ratio as a function of external magnetic field. The solid line represents the field-free switching ratio at different Ta thicknesses when there is zero magnetic field, and the dashed line is the in-plane auxiliary field when the polarity of SOT changes.

We further examined SOT efficiency of the trilayer structures by performing harmonic Hall voltage measurements. Figures 5(a) and 5(b) show the values of R_ω and $R_{2\omega}$ for the $t_{Ta} = 0.15$ nm sample as a typical example. A linear relationship between H_{DL} and the applied current at different t_{Ta} was observed and is shown in Fig. 5(c). The slope of this linear relationship is denoted by $\beta_{DL} = H_{DL}/J_c$, which is plotted for devices with different t_{Ta} in Fig. 5(d). We noticed that β_{DL} decreases gradually with increasing t_{Ta}, which is opposite to the trend of J_c changing with t_{Ta}. On the other hand, the current-induced SOT efficiency β_{DL} and the field-free switching ratio follow the exact same trend, which further confirms the influence of Ta thickness.

The IEC of two magnetic layers sandwiched by a Ta spacer is generally two or more orders weaker than that sandwiched by a Ru spacer, and depends on the materials used for the magnetic layers,[35,36] that is why very weak antiferromagnetic (AFM) coupling is observed in Co/Ta/Co while no AFM coupling is seen in Fe/Ta/Fe.[35] Although the 0.2 nm Pt layer between the Co and Ta in the studied (Co/Pt)/Ta/CoFeB trilayer is able to enhance the perpendicular anisotropy of the bottom Co layer, it further weakens the IEC, and therefore a Ta spacer of 0.5 nm is able to decouple the two magnetic layers (Co/Pt and CoFeB), resulting in two-step switching as observed in Figs. 2(a) and 3(b). Theoretically, the interlayer exchange field can be determined by the Ruderman–Kittel–Kasuya–Yosida formula

$$H_{\rm ex} \propto \sin(\phi + 2\pi t_{\rm Ta}/\lambda_{\rm F})/t_{\rm Ta}^2, \tag{2}$$

where $t_{\rm Ta}$ is the Ta spacer thickness. In the first FM coupling region, IEC decreases with increasing Ta thickness, approximately as $1/t_{\rm Ta}^2$.[36] Experimentally, a sharp decrease in FM IEC with increasing Ta spacer thickness has recently been reported for a Ta thickness ≤ 0.9 nm in an exchange-coupled CoFeB/Ta/CoFeB trilayer with in-plane and perpendicular anisotropy for the top and bottom magnetic layer, respectively.[37] The studied (Co/Pt)/Ta/CoFeB trilayer with Pt + Ta thickness ≤ 0.6 nm shows FM coupling, and the coupling strength should decrease with increasing Ta thickness as theoretically predicted and experimentally observed previously.

As the Ta spacer thickness varies, two things happen. The spin current generated by the Pt layer diffuses into the Co layer and passes through the Ta spacer into the top CoFeB layer, which exerts a torque on the CoFeB layer. As Ta is a heavy metal with strong spin–orbit coupling, spin reflection (backflow) (SBF) occurs at the (Co/Pt)/Ta interface, while spin memory loss (SML) happens both at the interface and when passing though the Ta spacer.[38] Therefore, the thicker the Ta spacer, the greater the SML. As a result of that, less spin current enters the CoFeB layer as the Ta spacer thickness increases, leading to less torque and a smaller SOT efficiency, as observed. On the other hand, as shown in Fig. 5(d), a three-times reduction of $\beta_{\rm DL}$, from 2.25 Oe/(10^7 A·cm^{-2}) to about 0.73 Oe/(10^7 A·cm^{-2}), is seen as the Ta spacer thickness increases from 0.15 nm (one sub-atomic layer) to 0.4 nm (about two atomic layers). SML only might not be able to fully account for the observed big decrease in $\beta_{\rm DL}$ as the Ta spacer thickness increases because it has little effect on the SOT acting on the Co layer, which should contribute more than half to the overall torque acting on the ferromagnetically coupled (Co/Pt)/Ta/CoFeB trilayer. Therefore, the IEC might play a partial role in the observed decrease in $\beta_{\rm DL}$. The main driving forces that act on the CoFeB layer and push its magnetization to switch are the current-induced damping-like torque and IEC-induced exchange torque that comes from exchange coupling with the bottom Co layer, and later decreases with the IEC. A reduced exchange torque demands higher damping to make the CoFeB layer switch happen, and equivalently reduces SOT efficiency. As discussed above, the IEC might decrease with Ta spacer thickness at $t_{\rm Ta} = 0.15$ nm–0.4 nm, and therefore might reduce $\beta_{\rm DL}$ as observed. That is, both the enhanced SML and reduced IEC cause the decrease in $\beta_{\rm DL}$ as Ta spacer thickness increases.

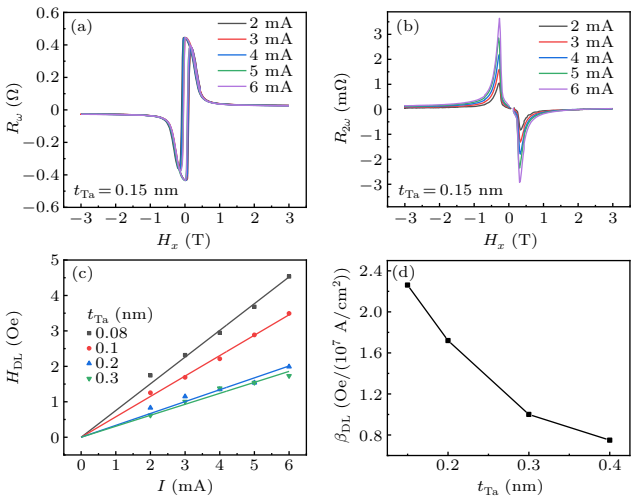


Fig. 5. (a) and (b) The first and second harmonic Hall resistances (R_ω and $R_{2\omega}$) as a function of in-plane magnetic field H_x for samples with different $t_{\rm Ta}$. The $R_{2\omega}$–H_x curves are fitted by Eq. (1). (c) Damping-like effective field $H_{\rm DL}$ versus applied AC for different Ta thicknesses. The solid lines are the fitting results. (d) $\beta_{\rm DL}$ as a function of $t_{\rm Ta}$.

In summary, the effect of Ta thickness on field-free switching and SOT efficiency in a ferromagnetically coupled Co/Ta/CoFeB trilayer with PMA was systematically investigated; this is different from previously reported works which are summarized in Table 1.

Table 1. FM/NM/FM trilayer research status.

System	Field-free switching	Coupling mode[a]	Magnetic anisotropy[b]	Reference
[Co/Pd]/Ru/[Co/Pd]	No	AFM	OP/OP	[39]
Co/Ru/Co/Ir/Co	No	AFM	IP/IP/OP	[40]
Co/CuIr/Co	No	AFM	IP/IP	[41]
Pt/Co/Ru/Co/Pt	No	FM	IP/IP	[42]
CoFe/Ru/CoFe/IrMn	Yes	AFM/FM	OP/IP	[26]
Pt/Co/IrMn	Yes	AFM	IP/OP	[19]
CoFeB/Ta/CoFeB	Yes	AFM	OP/IP	[22]
Co/Ta/Co	Yes	AFM	IP/OP	[43]
CoFeB/Ta/CoFeB	Yes	AFM	IP/OP	[44]
CoFeB/Ta/CoFeB	Yes	FM	OP/IP	[22]
CoFeB/Ta/CoFeB	Yes	FM	IP/OP	[37]
Co/Ta/CoFeB	Yes	FM	OP/OP	our work

[a]Antiferromagnetic (AFM) interlayer exchange coupling and ferromagnetic (FM) interlayer exchange coupling.
[b]Out-of-plane (OP) magnetizations and in-plane (IP) magnetizations.

4. Conclusion and perspectives

We systematically investigated the effect of Ta thickness on the magnetic properties, field-free switching and SOT efficiency in a ferromagnetically coupled Co/Ta/CoFeB trilayer with perpendicular magnetic anisotropy. We found that FM IEC happens in a narrow range of $0.15\ \text{nm} \leq t_{\text{Ta}} \leq 0.4\ \text{nm}$. The perpendicular easy axis disappears at $t_{\text{Ta}} < 0.15$ nm, while two layers are magnetically decoupled at $t_{\text{Ta}} \geq 0.5$ nm. The critical switching current density increases, while the field-free switching ratio and SOT efficiency decrease with increasing Ta thickness. Both the enhanced SML and reduced IEC cause a decrease in β_{DL} as Ta spacer thickness increases. In particular, the studied structure with the incorporation of a CoFeB layer is able to realize field-free switching in the strong FM coupling region, which may contribute to the future development of magnetic tunnel junctions for better memory applications.

Acknowledgments

Project supported by the 'Pioneer' and 'Leading Goose' Research and Development Program of Zhejiang Province, China (Grant No. 2022C01053), the National Natural Science Foundation of China (Grant Nos. 11874135, 12104119, and 12004090), Key Research and Development Program of Zhejiang Province, China (Grant No. 2021C01039), and Natural Science Foundation of Zhejiang Province, China (Grant Nos. LQ20F040005 and LQ21A050001).

References

[1] Liu L Q, Pai C F, Li Y, Tseng H W, Ralph D C and Buhrman R A 2012 *Science* **336** 555
[2] Liu L Q, Lee O J, Gudmundsen T J, Ralph D C and Buhrman R A 2012 *Phys. Rev. Lett.* **109** 096602
[3] Ando K, Takahashi S, Harii K, Sasage K, Ieda J, Maekawa S and Saitoh E 2008 *Phys. Rev. Lett.* **101** 036601
[4] Emori S, Bauer U, Ahn S M, Martinez E and Beach G S D 2013 *Nat. Mater.* **12** 611
[5] Haazen P P J, Mure E, Franken J H, Lavrijsen R, Swagten H J M and Koopmans B 2013 *Nat. Mater.* **12** 299
[6] Kimura T, Otani Y, Sato T, Takahashi S and Maekawa S 2007 *Phys. Rev. Lett.* **98** 156601
[7] Miron I M, Garello K, Gaudin G, Zermatten P J, Costache M V, Auffret S, Bandiera S, Rodmacq B, Schuhl A and Gambardella P 2011 *Nature* **476** 189
[8] Miron I M, Gaudin G, Auffret S, Rodmacq B, Schuhl A, Pizzini S, Vogel J and Gambardella P 2010 *Nat. Mater.* **9** 230
[9] Woo S, Mann M, Tan A J, Caretta L and Beach G S D 2014 *Appl. Phys. Lett.* **105** 212404
[10] Walker M R, Leung P, Eltahla A A, Underwood A, Abayasingam A, Brasher N A, Li H, Wu B R, Maher L, Luciani F, Lloyd A R and Bull R A 2019 *Sci. Rep.* **9** 13300
[11] Stamps R L, Breitkreutz S, Akerman J, Chumak A V, Otani Y, Bauer G E W, Thiele J U, Bowen M, Majetich S A, Klaui M, Prejbeanu I L, Dieny B, Dempsey N M and Hillebrands B 2014 *J. Phys. D: Appl. Phys.* **47** 333001
[12] Shao Q M, Yu G Q, Lan Y W, Shi Y M, Li M Y, Zheng C, Zhu X D, Li L J, Amiri P K and Wang K L 2016 *Nano Lett.* **16** 7514
[13] Du Y, Gamou H, Takahashi S, Karube S, Kohda M and Nitta J 2020 *Phys. Rev. Appl.* **13** 054014
[14] Razavi S A, Wu D, Yu G Q, Lau Y C, Wong K L, Zhu W H, He C L, Zhang Z Z, Coey J M D, Stamenov P, Amiri P K and Wang K L 2017 *Phys. Rev. Appl.* **7** 024023
[15] Wu H, Razavi S A, Shao Q M, Li X, Wong K L, Liu Y X, Yin G and Wang K L 2019 *Phys. Rev. B* **99** 184403
[16] Razavi A, Wu H, Shao Q M, Fang C, Dai B Q, Wong K, Han X F, Yu G Q and Wang K L 2020 *Nano Lett.* **20** 3703
[17] Fukami S, Zhang C L, DuttaGupta S, Kurenkov A and Ohno H 2016 *Nat. Mater.* **15** 535
[18] Oh Y W, Baek S H C, Kim Y M, Lee H Y, Lee K D, Yang C G, Park E S, Lee K S, Kim K W, Go G, Jeong J R, Min B C, Lee H W, Lee K J and Park B G 2016 *Nat. Nanotechnol.* **11** 878
[19] van den Brink A, Vermijs G, Solignac A, Koo J, Kohlhepp J T, Swagten H J M and Koopmans B 2016 *Nat. Commun.* **7** 10854
[20] Yu G Q, Upadhyaya P, Fan Y B, Alzate J G, Jiang W J, Wong K L, Takei S, Bender S A, Chang L T, Jiang Y, Lang M R, Tang J S, Wang Y, Tserkovnyak Y, Amiri P K and Wang K L 2014 *Nat. Nanotechnol.* **9** 548
[21] You L, Lee O, Bhowmik D, Labanowski D, Hong J, Bokor J and Salahuddin S 2015 *Proc. Natl. Acad. Sci. USA* **112** 10310
[22] Kong W J, Wan C H, Wang X, Tao B S, Huang L, Fang C, Guo C Y, Guang Y, Irfan M and Han X F 2019 *Nat. Commun.* **10** 233
[23] Shi G Y, Wan C H, Chang Y S, Li F, Zhou X J, Zhang P X, Cai J W, Han X F, Pan F and Song C 2017 *Phys. Rev. B* **95** 104435
[24] Wu H, Nance J, Razavi S A, Lujan D, Dai B Q, Liu Y X, He H R, Cui B S, Wu D, Wong K, Sobotkiewich K, Li X Q, Carman G P and Wang K L 2021 *Nano Lett.* **21** 515
[25] Fan H D, Luo Y M, Wu B R, Xu X Y, Zhuang Y S, Feng Z S, Li W J and Zhou T J 2022 *Phys. Rev. Lett.* **120** 142401
[26] Lau Y C, Betto D, Rode K, Coey J M D and Stamenov P 2016 *Nat. Nanotechnol.* **11** 758
[27] Sokalski V, Moneck M T, Yang E and Zhu J G 2012 *Appl. Phys. Lett.* **101** 072411
[28] Hayashi M, Kim J, Yamanouchi M and Ohno H 2014 *Phys. Rev. B* **89** 144425
[29] Roschewsky N, Lambert C H and Salahuddin S 2017 *Phys. Rev. B* **96** 064406
[30] Wu H, Xu Y, Deng P, Pan Q, Razavi S A, Wong K, Huang L, Dai B, Shao Q, Yu G, Han X, Rojas-Sanchez J C, Mangin S and Wang K L 2019 *Adv. Mater.* **31** 1901681
[31] Razavi A, Wu H, Dai B, He H, Wu D, Wong K, Yu G and Wang K L 2020 *Appl. Phys. Lett.* **117** 182403
[32] Zheng Z Y, Zhang Y, Lopez V, Sanchez-Tejerina L, Shi J C, Feng X Q, Chen L, Wang Z L, Zhang Z Z, Zhang K, Hong B, Xu Y, Zhang Y G, Carpentieri M, Fert A, Finocchio G, Zhao W S and Amiri P K 2021 *Nat. Commun.* **12** 4555
[33] Frackowiak L, Stobiecki F, Urbaniak M, Matczak M, Chaves-O Flynn G D, Bilski M, Glenz A and Kuswik P 2022 *J. Magn. Magn. Mater.* **544** 168682
[34] Shu X Y, Liu L, Zhou J, Lin W N, Xie Q D, Zhao T Y, Zhou C H, Chen S H, Wang H, Chai J W, Ding Y S, Chen W and Chen J S 2022 *Phys. Rev. Appl.* **17** 024031
[35] Parkin S S P 1991 *Phys. Rev. Lett.* **67** 3598
[36] Parkin S S P and Mauri D 1991 *Phys. Rev. B* **44** 7131
[37] Lazarski S, Skowronski W, Grochot K, Powroznik W, Kanak J, Schmidt M and Stobiecki T 2021 *Phys. Rev. B* **103** 134421
[38] Zhu L and Buhrman R A 2019 *Phys. Rev. Appl.* **12** 051002
[39] Zhang P X, Liao L Y, Shi G Y, Zhang R Q, Wu H Q, Wang Y Y, Pan F and Song C 2018 *Phys. Rev. B* **97** 214403
[40] Liu Y, Zhou B and Zhu J G 2019 *Sci. Rep.* **9** 325
[41] Masuda H, Seki T, Lau Y C, Kubota T and Takanashi K 2020 *Phys. Rev. B* **101** 224413
[42] Dai Z M, Liu W, Zhao X T, Liu L and Zhang Z D 2021 *ACS Appl. Electron. Mater.* **3** 611
[43] Sheng Y, Edmonds K W, Ma X Q, Zheng H Z and Wang K Y 2018 *Adv. Electron. Mater.* **4** 1800224
[44] Zhang R Q, Shi G Y, Su J, Shang Y X, Cai J W, Liao L Y, Pan F and Song C 2020 *Appl. Phys. Lett.* **117** 212403